SIGNAL AND NOISE ANALYSIS OF EXTERNAL MODULATION FIBER OPTIC LINK WITH OPTICAL COMPONENT AND ARBITRARY LOSSLESS MATCHING CIRCUITS

E. I. Ackerman, J. L. Prince, and J. A. MacDonald

Martin Marietta Laboratories•Syracuse
Electronics Park, Syracuse, New York 13221

ABSTRACT

We present and experimentally verify a general analytical signal and noise model for an external modulation fiber optic link that includes an optical component with gain or loss, and arbitrary lossless matching circuits at the input and output.

I. INTRODUCTION

System designers must know the impact of fiber optic link signal and noise behavior if such links are to replace conventional metallic waveguides in radar and communications antenna remoting applications. An RF fiber optic link consists of several active devices, including an optical source and electro-optic modulator (a single device in the case of a directly-modulated semiconductor laser, or a separate source and external modulator) and a high-speed photodetector. It may also include other optical components such as polarizers, isolators, optical amplifiers, and filters. Each optical component affects the signal and noise performance of the link.

Cox et al. [1] derived a set of signal and noise equations for a lumped-element modulator-based external modulation link with optimum single-frequency matching circuits at the input and output, which leads to a minimum noise figure of 2 (3 dB). Betts and O'Donnell [2] later showed the minimum noise figure could be reduced below 3 dB by "de-tuning" the lumped-element modulator matching at the expense of some link gain. Experimental results in both cases were at frequencies below 1 GHz. For higher frequencies, use of a traveling-wave modulator results in better link performance [3].

In this paper, we give a general analytical model of the gain, noise power, and noise figure of an external modulation fiber optic link using arbitrary lossless (reactive) networks at the traveling-wave external modulator input and detector output. The model includes the detector thermal noise contribution to link noise figure. In external modulation links employing low-noise solid-state lasers, it is often the detector thermal noise that dominates the link's output noise power (and thus its noise figure). The model also accommodates a general two-port optical component represented by its gain G_o, noise figure F_o, and bandwidth B_o. This two-port can consist of: an active device such as an optical amplifier; a spectrum-modifying device such as an optical filter; a passive optical component with loss, in which case its noise figure F_o equals its loss $1/G_o$, or; a combination of such devices, in which case calculation of the total cascaded gain and noise figure depends on minimization of optical reflections in the chain.

TH 2D

II. LINK EQUIVALENT CIRCUIT

Figure 1 shows the fiber optic link equivalent circuit model used as the basis for our analysis. The modulator's traveling-wave electrodes have length L_e, characteristic impedance Z_c, and termination impedance Z_t. A lossless circuit with loaded current transfer function $H_M(\omega)$ resides between the RF source and the modulator electrodes. From its loaded input and output ends this circuit has impedances $Z_{M,i}(\omega)$ and $Z_{M,o}(\omega)$, respectively. A signal voltage source $V_{in,rms}$ with impedance Z_{in} drives the modulator. With the real part of Z_{in} is associated a mean square noise voltage $\langle E_{in}^2 \rangle$, where:

$$\langle E_{in}^2 \rangle = 4\,k\,T\,B\,R_{in}\,. \qquad (1)$$

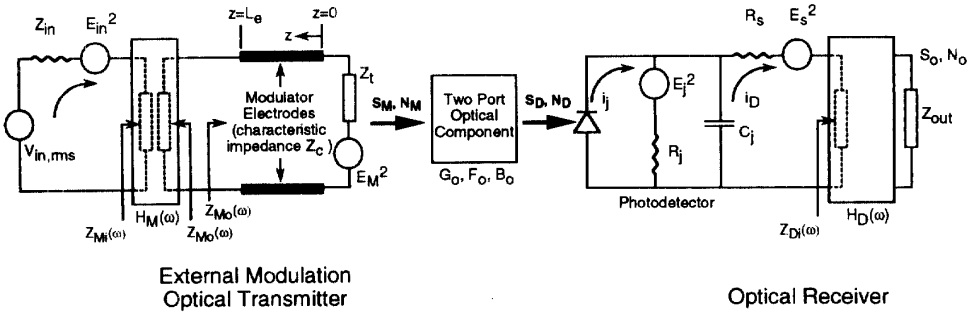

Figure 1 External modulation link equivalent model including two-port optical component and loaded current transfer functions $H_M(\omega)$ and $H_D(\omega)$.

CH3577-4/95/0000-1173$01.00 © 1995 IEEE

In (1), k is Boltzmann's constant, T is the absolute temperature, B is the electrical bandwidth, and R_{in} is the real part of Z_{in}. Likewise, with the real part of the modulator termination impedance is associated another thermal mean-square noise voltage $\langle E_M^2 \rangle$ calculated similarly. A paper presented in 1994 [4] explained all other terms shown the Figure 1 model.

III. SIGNAL ANALYSIS

For small RF signals, the magnitude of RF modulation on the optical output of a Mach-Zehnder interferometric modulator is:

$$S_M(\omega) = \frac{\pi}{2}\,\alpha_{opt}\,P_L\,\frac{v_M(\omega)}{V_\pi(\omega)}\cos\left(\frac{\pi\,V_b}{V_{\pi(DC)}}\right). \tag{2}$$

The last term in (2) is somewhat different for directional and y-fed coupler modulators [5]. V_b is the difference between the DC bias voltage and the quarterwave DC bias voltage (so that V_b=0 defines the quarterwave bias point), α_{opt} is the optical insertion loss of the modulator, and P_L is the laser optical power available at the modulator's optical input. V_π is the halfwave on-off switching voltage, which is different at DC than at high frequencies due in part to velocity mismatch between the RF signals in the electrical and optical waveguides. Defining the normalized velocity mismatch as δ, the frequency dependent halfwave voltage can be calculated as follows [3]:

$$V_\pi(\omega) = \frac{2\pi\,\lambda_{opt}\,G_e}{n_o^3\,r_{ij}\,\Gamma_{eo}}\,\frac{Z_M(\omega,L_e)}{\displaystyle\int_0^{L_e} Z_M(\omega,z)\cos\beta\delta z\,dz}. \tag{3}$$

In (3), G_e, n_o, r_{ij}, Γ_{eo}, and β, are the modulator's coplanar electrode gap, effective optical waveguide index, electro-optic tensor, electrical-optical field overlap integral, and lossless microwave propagation constant, respectively, and λ_{opt} is the optical wavelength. $Z_M(\omega,z)$ is the modulator impedance at the RF frequency as seen from a distance z from the termination load Z_t, and can be approximated as follows for devices with relatively short or low-loss traveling-wave electrodes [6]:

$$Z_M(\omega,z) = Z_c\,\frac{Z_t + j\,Z_c\tan\beta z}{Z_c + j\,Z_t\tan\beta z}. \tag{4}$$

The transducer gain, G_t, of the link is the ratio of power delivered to the load to power available from the RF source. Using the equivalent circuit shown, the derivation yields [4]:

$$G_t = \frac{\pi^2\,\eta_D^2\,|H_M|^2\,|H_D|^2\,\alpha_{opt}^2\,G_o^2\,P_L^2\,|Z_{ei}|^2\,R_{in}\,R_{out}\,|Z_M(\omega,L_e)|^2}{V_\pi^2(\omega)\,|R_S+Z_{ei}+Z_{Di}|^2\,|Z_{in}+Z_{Mi}|^2}$$

$$\times\cos^2\left(\frac{\pi\,V_b}{V_{\pi(DC)}}\right), \tag{5}$$

where R_{out} is the real part of Z_{out}, and where:

$$Z_{ei}(\omega) = \frac{R_j}{1 + j\,\omega\,R_j\,C_j}. \tag{6}$$

IV. NOISE ANALYSIS

Six terms contribute to the noise power N_o at the link output:

$$N_o = kTB\,G_t + \frac{kTB\,G_t\,|Z_{in}+Z_{Di}|^2\,|Z_M(\omega,L_e)|}{|Z_M(\omega,L_e)+Z_{Mo}|^2\,|H_M|^2\,R_{in}}$$

$$+\frac{RIN\,B\,G_t\,|Z_{in}+Z_{Mi}|^2\,V_\pi^2(\omega)}{4\,\pi^2\,|Z_M(\omega,L_e)|^2\,|H_M|^2\,R_{in}}\left[\frac{1+\sin\dfrac{\pi\,V_b}{V_{\pi(DC)}}}{1-\sin\dfrac{\pi\,V_b}{V_{\pi(DC)}}}\right]$$

$$+\frac{(kTB_o)^2\,G_t\,(F_o-1)^2\,|Z_{in}+Z_{Di}|^2\,V_\pi^2(\omega)}{\pi^2\,|H_M|^2\,\alpha_{opt}^2\,P_L^2\,|Z_M(\omega,L_e)|^2\,R_{in}\cos^2\dfrac{\pi\,V_b}{V_{\pi(DC)}}}$$

$$+\frac{q\,|Z_{in}+Z_{Di}|^2\,V_\pi^2(\omega)\,B\,G_t\left[1-\sin\dfrac{\pi\,V_b}{V_{\pi(DC)}}\right]^{-1}}{\pi^2\,\alpha_{opt}\,G_o\,\eta_D\,|H_M|^2|Z_M(\omega,L_e)|^2\,R_{in}\,P_L} \tag{7}$$

$$+\frac{4\,kTB\,G_t\,V_\pi^2(\omega)\,|Z_{in}+Z_{Mi}|^2\left[1+\dfrac{R_s}{R_j}+\omega^2C_j^2R_sR_j\right]}{\pi^2\,\alpha_{opt}^2G_o^2\,P_L^2\,\eta_D^2\,|H_M|^2|Z_M(\omega,L_e)|^2R_{in}R_j\cos^2\dfrac{\pi\,V_b}{V_{\pi(DC)}}}.$$

The first term in equation (7) represents thermal noise at the output due to the input terminals. The second term is the thermal noise contribution from the modulator termination impedance. The third term arises from the detected relative intensity noise (RIN) output of the optical source. The fourth term is the detected noise generated by the optical component; the noise figure and optical bandwidth of the optical component appear in this term, and can be sufficiently large to cause the noise power due to this component to dominate the link noise figure. The fifth and sixth terms are the shot noise and detector thermal noise contributions, respectively.

The noise figure F, defined as signal-to-noise ratio degradation in the link for an input thermal noise of kTB, is therefore:

$$F = 1 + \frac{|Z_{in}+Z_{Di}|^2\,|Z_M(\omega,L_e)|}{|Z_M(\omega,L_e)+Z_{Mo}|^2\,|H_M|^2\,R_{in}}$$

$$+\frac{RIN\,|Z_{in}+Z_{Mi}|^2\,V_\pi^2(\omega)}{4\,kT\,\pi^2\,|Z_M(\omega,L_e)|^2\,|H_M|^2\,R_{in}}\left[\frac{1+\sin\dfrac{\pi\,V_b}{V_{\pi(DC)}}}{1-\sin\dfrac{\pi\,V_b}{V_{\pi(DC)}}}\right]$$

$$+\frac{kT\,B_o^2\,(F_o-1)^2\,|Z_{in}+Z_{Di}|^2\,V_\pi^2(\omega)}{B\,\pi^2\,|H_M|^2\,\alpha_{opt}^2\,P_L^2\,|Z_M(\omega,L_e)|^2\,R_{in}\cos^2\dfrac{\pi\,V_b}{V_{\pi(DC)}}}$$

$$+\frac{q\,|Z_{in}+Z_{Mi}|^2\,V_\pi^2(\omega)\left[1-\sin\dfrac{\pi\,V_b}{V_{\pi(DC)}}\right]^{-1}}{kT\,\pi^2\,\alpha_{opt}\,G_o\,\eta_D\,|H_M|^2|Z_M(\omega,L_e)|^2\,R_{in}\,P_L} \tag{8}$$

$$+\frac{4\,V_\pi^2(\omega)\,|Z_{in}+Z_{Mi}|^2\left[1+\dfrac{R_s}{R_j}+\omega^2C_j^2R_sR_j\right]}{\pi^2\,\alpha_{opt}^2G_o^2\,P_L^2\,\eta_D^2\,|H_M|^2|Z_M(\omega,L_e)|^2R_{in}R_j\cos^2\dfrac{\pi\,V_b}{V_{\pi(DC)}}}.$$

A. Optimally Matched Input/Output Circuits

If the link is ideally matched at a single frequency, then:

$$|H_M|^2 = \frac{Z_0}{Z_M(\omega,L_e)}\,;|H_D|^2 = \frac{R_s}{Z_0}\,,\ \text{and;}\ R_{in} = R_{out} = Z_0\,. \quad (9)$$

If the detector junction resistance R_j is assumed to be infinite for all practical purposes, then equations (5) and (8) reduce to:

$$G_t = \frac{\pi^2\,\eta_D^2\,\alpha_{opt}^2 G_o^2\,P_L^2\,|Z_M(\omega,L_e)|\cos^2\left(\frac{\pi\,V_b}{V_\pi(DC)}\right)}{16\,\omega^2\,C_j^2\,R_s\,V_\pi^2(\omega)} \quad (10)$$

and

$$F = 2 + \frac{RIN\,V_\pi^2(\omega)}{kT\,\pi^2\,|Z_M(\omega,L_e)|}\left[\frac{1+\sin\frac{\pi\,V_b}{V_\pi(DC)}}{1-\sin\frac{\pi\,V_b}{V_\pi(DC)}}\right]$$

$$+\frac{4\,kT\,B_o^2\,(F_o-1)^2\,V_\pi^2(\omega)}{B\,\pi^2\,\alpha_{opt}^2\,P_L^2\,|Z_M(\omega,L_e)|\cos^2\frac{\pi\,V_b}{V_\pi(DC)}}$$

$$+\frac{4\,q\,V_\pi^2(\omega)\left[1-\sin\frac{\pi\,V_b}{V_\pi(DC)}\right]^{-1}}{kT\,\pi^2\,\alpha_{opt}\,G_o\,\eta_D\,|Z_M(\omega,L_e)|\,P_L}+\frac{1}{G_t}\,. \quad (11)$$

B. Quarterwave Bias Point

Equations (5) and (10) show that G_t is maximum when the modulator is biased at the quarterwave bias $V_b=0$. Examination of equations (8) and (11), however, shows that the bias for lowest noise figure can occur between the quarterwave and pinch-off voltages (0 and $-V_\pi(DC)/2$, respectively). The complexity of external modulation link performance dependence on modulator DC bias was discussed in another paper [7]; in this paper we proceed assuming operation at the quarterwave bias point, which simplifies equations (5)–(11).

C. Balanced Receiver Architecture

Using a modulator of either the directional- or y-fed coupler variety, both of which have two optical fiber outputs, it is possible to construct a link using a balanced receiver in which the signal components of the two optical fibers add up constructively while the noise components add up destructively. This link architecture has zero output noise due to laser RIN when perfect balancing is achieved and the modulator is operated at its quarterwave bias voltage [8]. Consequently, low external modulation link noise figure does not require a low-RIN solid-state laser such as a Nd:YAG. A comparatively small and inexpensive semiconductor laser (which can be integrated into the modulator package) can be used to achieve the same gain and noise figure (if P_L is the same):

$$G_{t,bal} = \frac{\pi^2\,\eta_D^2\,\alpha_{opt}^2 G_o^2\,P_L^2\,|Z_M(\omega,L_e)|}{4\,\omega^2\,C_j^2\,R_s\,V_\pi^2(\omega)} \quad (12)$$

at $V_b=0$ for perfect balancing, and:

$$F_{bal} = 2 + \frac{4\,q\,V_\pi^2(\omega)}{kT\,\pi^2\,\alpha_{opt}\,G_o\,\eta_D\,|Z_M(\omega,L_e)|\,P_L} + \frac{2}{G_t}\,. \quad (13)$$

V. EXPERIMENTAL VERIFICATION OF MODEL

In [4] we experimentally verified that the equivalent circuit modeling technique we employ accounts for the effect upon link performance of ideal impedance matching at a single frequency vs. non-ideal matching across a broad band vs. no impedance matching. We also measured the effects of optical component gain, noise figure, and bandwidth on link performance and proved our model's ability to predict these effects. Moreover, the measured impact of using the balanced receiver architecture to cancel detected RIN was shown in [8] to verify our predictions. What remains is to prove that the model given by equations (1)-(11) reflects the complex extent to which external modulation link performance depends on the optical power illuminating the detector.

To experimentally verify this aspect of our model, we constructed an external modulation link using the following components: an AMOCO Nd:YAG (λ=1.3μm) laser with single-mode output fiber pigtail; a JDS Fitel variable optical attenuator; a polarization rotator; a single-output United Technologies Photonics y-fed coupler traveling-wave modulator, and; a single Epitaxx InGaAs p-i-n backfacet-illuminated photodiode reactively matched to 50 Ω at 10 GHz.

We selected the Nd:YAG laser in our experimental link not for its low RIN but rather for its high optical power output. Using this laser in conjunction with the precisely variable optical attenuator allowed us to measure link performance at detector illumination levels ranging from less than –50 dBm up to the detector's damage threshold (about +8 dBm).

In Figure 2 we show the modeled effect of detected optical power upon external modulation link output signal and noise powers at 10 GHz, predicted by substituting the listed device parameters into equations (5) and (8). Measured data points are also plotted at selected detector illumination levels (shown as triangles), showing excellent agreement with the model. The portion of the signal-to-noise ratio curve having a slope of 2 corresponds to detector illumination levels at which the output thermal noise power limits the link dynamic range.

At the very high input powers (up to +10 dBm), the RIN of the laser limits the dynamic range, resulting in a flattening of the signal-to-noise ratio curve because the RIN noise and the gain increase at the same rate with respect to detector illumination. The laser we used had a higher RIN at 10 GHz (-155 dB/Hz) than some YAG lasers. For lower-RIN (<-160 dB/Hz) lasers, the upper end of the curve would be shot-noise limited and would have a slope of 1. The difference between the measured and modeled data is probably due to the fact that we modeled the modulator traveling-wave electrodes as a lossless transmission line when in fact the 10 GHz attenuation is probably fairly substantial.

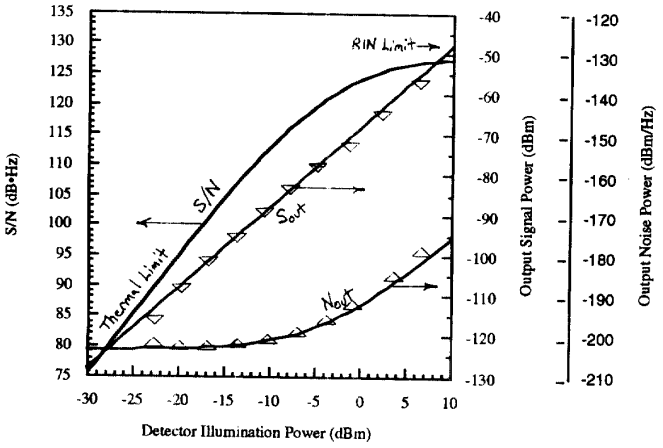

Measured Device Parameters	
Input 10 GHz Signal Power	0 dBm
η_D	0.8 A/W
α_{opt}	-2.3 dB
G_o	variable
P_L	12.5 dBm
$\|Z_M(\omega,L_e)\|$	31 Ω
f	10 GHz
C_j	0.25 pF
R_s	9 Ω
$V_\pi(\omega)$	12.5 V
RIN	-155 dB/Hz at 10 GHz
kT	-173.8 dBm/Hz

Figure 2 Measured and predicted signal and noise power, and signal-to-noise ratio for experimental link at 10 GHz, as a function of detected optical power.

REFERENCES

[1] C. H. Cox, L. M. Johnson, and G. E. Betts, "A Theoretical and Experimental Comparison of Directly and Externally Modulated Fiber-Optic Links," *1989 IEEE MTT-S Symposium Digest*, pp. 689-672.

[2] G. E. Betts and F. J. O'Donnell, "Improvements in Passive, Low-Noise-Figure Optical Links," *1993 ARPA Symposium on Photonics Systems for Antenna Applications (Technical Program).*

[3] R. C. Alferness, "Waveguide Electrooptic Modulators," IEEE Transactions on Microwave Theory and Techniques, Vol. MTT-30, No. 8, August 1982, pp. 1121-1137.

[4] J. A. MacDonald, E. I. Ackerman, and J. L. Prince, "Signal and Noise Analysis of Direct Modulation Fiber Optic Link with Optical Component and Arbitrary Lossless Matching Circuits," *1994 MTT-S Symposium Digest*, pp. 167-170.

[5] M. T. Abuelma'atti, "Large Signal Analysis of Optical Directional Coupler Modulators," IEEE Transactions on Microwave Theory and Techniques," Vol. 40, No. 8, pp. 1722-1725.

[6] R. E. Collin, *Foundations for Microwave Engineering*, McGraw-Hill, Inc., New York, 1966, pp. 180-181.

[7] E. Ackerman, S. Wanuga, D. Kasemset, A. Daryoush, and N. Samant, "Maximum Dynamic Range Operation of a Microwave External Modulation Fiber-Optic Link," IEEE Transactions on Microwave Theory and Techniques, Vol. MTT-41, No. 8, pp. 1299-1306.

[8] E. Ackerman, S. Wanuga, J. MacDonald, and J. Prince, "Balanced Receiver External Modulation Fiber-Optic Link Architecture with Reduced Noise Figure," *1993 IEEE MTT-S Symposium Digest*, pp. 723-726.